A vector-free microfluidic platform for intracellular delivery

Armon Sharei[a,b,1], Janet Zoldan[b,1], Andrea Adamo[a,1], Woo Young Sim[a], Nahyun Cho[a], Emily Jackson[a], Shirley Mao[a], Sabine Schneider[c], Min-Joon Han[d], Abigail Lytton-Jean[b], Pamela A. Basto[e], Siddharth Jhunjhunwala[b], Jungmin Lee[f], Daniel A. Heller[b,g], Jeon Woong Kang[h], George C. Hartoularos[a], Kwang-Soo Kim[d], Daniel G. Anderson[a,b], Robert Langer[a,b,2], and Klavs F. Jensen[a,2]

Departments of [a]Chemical Engineering, [c]Biology, and [f]Chemistry, [b]The David H. Koch Institute for Integrative Cancer Research, [e]Division of Health Science and Technology, and [h]Laser Biomedical Research Center, G. R. Harrison Spectroscopy Laboratory, Massachusetts Institute of Technology, Cambridge, MA 02139; [d]Molecular Neurobiology Laboratory, Department of Psychiatry, Program in Neuroscience and Harvard Stem Cell Institute, McLean Hospital/Harvard Medical School, Belmont, MA 02478; and [g]Molecular Pharmacology and Chemistry Program, Memorial Sloan-Kettering Cancer Center, New York, NY 10065

Edited* by David A. Tirrell, California Institute of Technology, Pasadena, CA, and approved December 21, 2012 (received for review October 25, 2012)

Intracellular delivery of macromolecules is a challenge in research and therapeutic applications. Existing vector-based and physical methods have limitations, including their reliance on exogenous materials or electrical fields, which can lead to toxicity or off-target effects. We describe a microfluidic approach to delivery in which cells are mechanically deformed as they pass through a constriction 30–80% smaller than the cell diameter. The resulting controlled application of compression and shear forces results in the formation of transient holes that enable the diffusion of material from the surrounding buffer into the cytosol. The method has demonstrated the ability to deliver a range of material, such as carbon nanotubes, proteins, and siRNA, to 11 cell types, including embryonic stem cells and immune cells. When used for the delivery of transcription factors, the microfluidic devices produced a 10-fold improvement in colony formation relative to electroporation and cell-penetrating peptides. Indeed, its ability to deliver structurally diverse materials and its applicability to difficult-to-transfect primary cells indicate that this method could potentially enable many research and clinical applications.

drug delivery | induced pluripotent stem cells | reprogramming | protein delivery | nanoparticle delivery

Intracellular delivery of macromolecules is a critical step in therapeutic and research applications. Nanoparticle-mediated delivery of DNA and RNA, for example, is being explored for gene therapy (1, 2), while protein delivery is a promising means of affecting cellular function in both clinical (3) and laboratory (4) settings. Other materials, such as small molecules, quantum dots, or gold nanoparticles, are of interest for cancer therapies (5, 6), intracellular labeling (7, 8), and single-molecule tracking (9).

The cell membrane is largely impermeable to macromolecules. Many existing techniques use polymeric nanoparticles (10, 11), liposomes (12), or chemical modifications of the target molecule (13), such as cell-penetrating peptides (CPPs) (14, 15), to facilitate membrane poration or endocytotic delivery. In these methods, the delivery vehicle's efficacy is often dependent on the structure of the target molecule and the cell type. These methods are thus efficient in the delivery of structurally uniform materials, such as nucleic acids, but often ill-suited for the delivery of more structurally diverse materials, such as proteins (16, 17) and some nanomaterials (7). Moreover, the endosome escape mechanism that most of these methods rely on is often inefficient; hence, much material remains trapped in endosomal and lysosomal vesicles (18). More effective gene delivery methods, such as viral vectors (19, 20), however, often risk chromosomal integration and are limited to DNA and RNA delivery.

Membrane poration methods, such as electroporation (21, 22) and sonoporation (23), are an attractive alternative in some applications. Indeed, electroporation has demonstrated its efficacy in a number of DNA (24) and RNA (25) delivery applications for previously difficult-to-transfect primary cells. However, this method can cause cell death and has been shown to damage sensitive materials such as quantum dots, which aggregate due to exposure to electric fields (8). There have also been limited reports of successful protein delivery by this mechanism (26, 27). Microinjection, is perhaps the most direct method of delivering material to the cell cytoplasm regardless of cell type or delivery material. Although effective for certain applications, such as producing transgenic organisms, the method's low throughput is a disadvantage in many therapeutic and research applications (28, 29).

In this article, we describe a method for cytosolic delivery based on rapid mechanical deformation of the cell to produce transient membrane disruptions that facilitate the passive diffusion of material into the cell cytosol. This method was developed with the aim of delivering almost any macromolecule of interest to almost any cell type, at high throughput. Although scrape loading and shear-based delivery methods have been demonstrated previously, they are unsuitable for some applications due to low viability and/or delivery efficiency (30–32). However, such injury/diffusion-based delivery methods do have the advantage of high throughput (compared with microinjection) and independence from exogenous materials or fields. Our proposed technique is distinct from previous methods because it uses a physical constriction to deform and shear the cells in a controlled, reproducible manner, thus minimizing cell death while allowing one to optimize for delivery efficiency. Unlike the aforementioned delivery methods, this approach does not rely on electric fields, exogenous materials, endocytosis, or chemical modification of the target molecule. Our data indicate that this method could be particularly advantageous for applications involving nanomaterials, proteins, or difficult-to-transfect cell types, such as immune cells and stem cells—all of which are often underserved by current methods.

Results

Delivery Method. We hypothesize that the rapid mechanical deformation of a cell, as it passes through a constriction with a minimum dimension smaller than the cell diameter, results in the formation of transient membrane disruptions or holes (Fig. 1*A*). The size and frequency of these holes would be a function of the shear and compressive forces experienced by the cell during its passage through the constriction. Material from the surrounding medium may then diffuse directly into the cell cytosol throughout

Author contributions: A.S., J.Z., A.A., M.-J.H., A.L.-J., P.A.B., K.-S.K., D.G.A., R.L., and K.F.J. designed research; A.S., J.Z., A.A., W.Y.S., N.C., E.J., S.M., S.S., M.-J.H., A.L.-J., P.A.B., S.J., J.W.K., and G.C.H. performed research; M.-J.H., J.L., D.A.H., J.W.K., and K.-S.K. contributed new reagents/analytic tools; A.S., J.Z., N.C., E.J., S.S., M.-J.H., A.L.-J., D.A.H., and J.W.K. analyzed data; and A.S., R.L., and K.F.J. wrote the paper.

The authors declare no conflict of interest.

*This Direct Submission article had a prearranged editor.

[1]A.S., J.Z., and A.A. contributed equally to this work.

[2]To whom correspondence may be addressed. E-mail: kfjensen@mit.edu or rlanger@mit.edu.

This article contains supporting information online at www.pnas.org/lookup/suppl/doi:10.1073/pnas.1218705110/-/DCSupplemental.

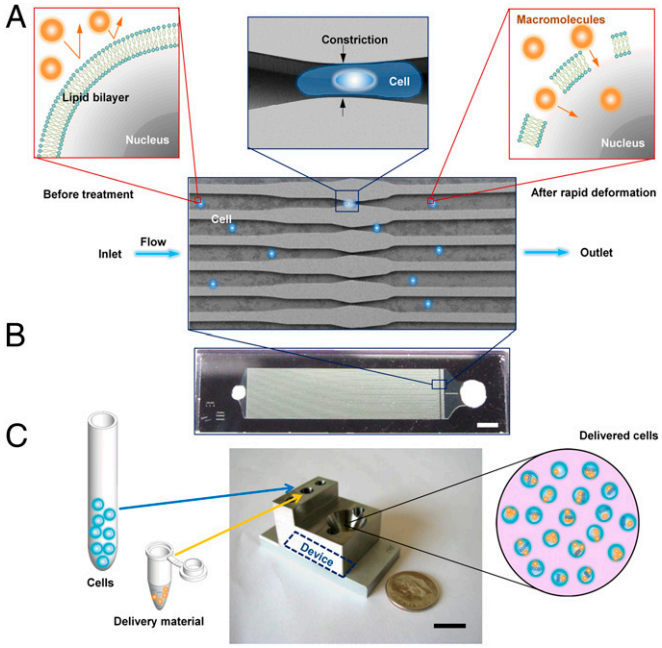

Fig. 1. Delivery mechanism and system design. (*A*) Illustration of delivery hypothesis whereby the rapid deformation of a cell, as it passes through a microfluidic constriction, generates transient membrane holes. Includes an electron micrograph of current parallel channel design with blue cells as an illustration. (*B*) Image of a finished device consisting of Pyrex bound to silicon for sealing. (Scale bar: 2 mm.) (*C*) Illustration of the delivery procedure in which cells and delivery material are mixed in the inlet reservoir, run through the chip, and collected in the outlet reservoir. The mounting system consists of stainless-steel and aluminum parts interfaced to the chip by inert O rings. (Scale bar: 10 mm.)

the life span of these holes. Such an approach could theoretically enable the diffusive delivery of any macromolecule small enough to fit through the holes. To implement this approach, we generated a family of microfluidic devices with different constriction dimensions and numbers of constrictions in series.

Each device (Fig. 1*B*) consists of 45 identical, parallel microfluidic channels, containing one or more constrictions, etched onto a silicon chip and sealed by a Pyrex layer. The width and length of each constriction (defined in Fig. S1) range from 4 to 8 μm and 10 to 40 μm, respectively. The current design is typically operated at a throughput rate of 20,000 cells/s, yielding close to 1 million treated cells per device before failure by clogging. The parallel channel design was chosen to increase throughput, while ensuring uniform treatment of cells, because any clogging or defects in one channel cannot affect the flow speed in neighboring channels (the device is operated at constant pressure). Before use, the device is first connected to a steel interface (Fig. 1*C*) that connects the inlet and outlet reservoirs to the silicon device. A mixture of cells and the desired delivery material is then placed into the inlet reservoir and Teflon tubing is attached at the inlet. A pressure regulator is then used to adjust the pressure at the inlet reservoir and drive the cells through the device. Treated cells are collected from the outlet reservoir.

Governing Parameters. We identified cell speed, constriction dimensions, and number of constrictions as three parameters that influence delivery efficiency (defined as the fraction of live cells that receive the delivery material; Fig. S1) by altering the shear and compression rates experienced by the cells. For example, delivery efficiency of membrane-impermeable, Cascade Blue-labeled 3-kDa dextran molecules to live HeLa cells increases monotonically with cell speed across different constriction designs (Fig. 2*A*). Constriction dimensions also impact delivery; increasing the constriction length from 20 to 40 μm almost doubled delivery efficiency at all operating speeds (Fig. 2*A*), with minimal effect on viability (Fig. 2*B*). Decreasing constriction width had a similar effect (Fig. S2*A*). Increasing the number of constrictions in series also increased delivery efficiency such that a device with five 10-μm length constrictions in series outperformed a single 10-, 20-, or 40-μm length design across all cell speeds (Fig. 2 *A* and *B*). One could also treat cells multiple times using the same device to enhance delivery, although this can lead to significant loss in viability. In these data, the 0 mm/s data points correspond to our control case whereby the cells undergo the same treatment as the other samples but are not passed through the device, thus reflecting any endocytotic or surface binding effects.

Cytosolic Delivery by Diffusion. As the majority of current nanoparticle and CPP-based delivery techniques are predicted to exploit endocytotic pathways (33), we sought to rule out the influence of endocytosis in our delivery mechanism. Confocal microscopy of cells treated with Cascade Blue-conjugated 3-kDa dextran demonstrate diffuse cytosolic staining (Fig. 3*A*) as opposed to the punctate characteristic one would expect of endocytotic methods (7). Moreover, when delivery experiments are conducted at 4 °C, a temperature at which endocytosis is minimized (34), delivery efficiency is minimally affected by temperature for both 3- and 70-kDa dextran (Fig. S2*B*). These data indicate that endocytosis is unlikely to be responsible for delivery in this system.

To test our diffusive delivery hypothesis, we characterized the delivery kinetics over time. In this experiment, cells were treated by the device in the absence of delivery material and subsequently exposed to Cascade Blue-labeled 3-kDa dextran at defined time intervals after treatment. The results indicate that 70–90% of delivery occurs within the first minute after treatment regardless of device design (Fig. 3*B*). The observed timescale supports the hole formation hypothesis as previous works on membrane repair kinetics have reported membrane sealing occurring at about 30 s after an injury is induced (35).

If delivery of material through the membrane disruptions is diffusive, material could be exchanged into and out of the cell throughout the lifetime of the hole. To demonstrate bidirectional transport of material across the cell membrane, we conducted an experiment consisting of three delivery cycles. Cells were first treated in the presence of 3- and 70-kDa dextran (cycle 1), washed

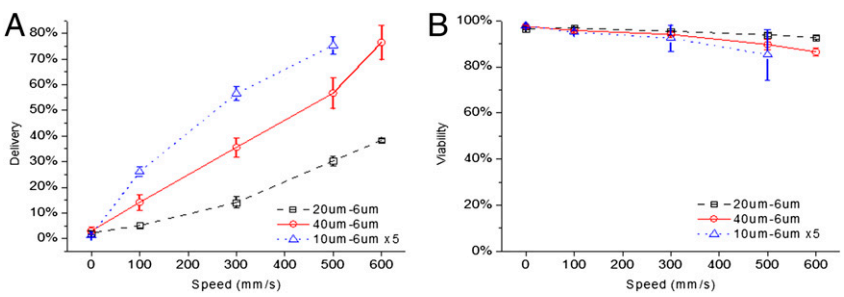

Fig. 2. Delivery performance depends on cell speed and constriction design. Constriction dimensions (Fig. S1) are denoted by numbers (e.g., 10 μm – 6 μm × 5) such that the first number corresponds to constriction length, the second to constriction width and the third (if present) to the number of constrictions in series per channel. (*A*) Delivery efficiency and (*B*) cell viability 18 h after treatment as a function of cell speed for 40 μm – 6 μm (○), 20 μm – 6 μm (□), and 10 μm – 6 μm × 5 (△) device designs. Efficiencies and viabilities were measured by flow cytometry after propidium iodide staining. For information regarding cell recovery rates, refer to *SI Note S1*. All data points were run in triplicate, and error bars represent 2 SDs.

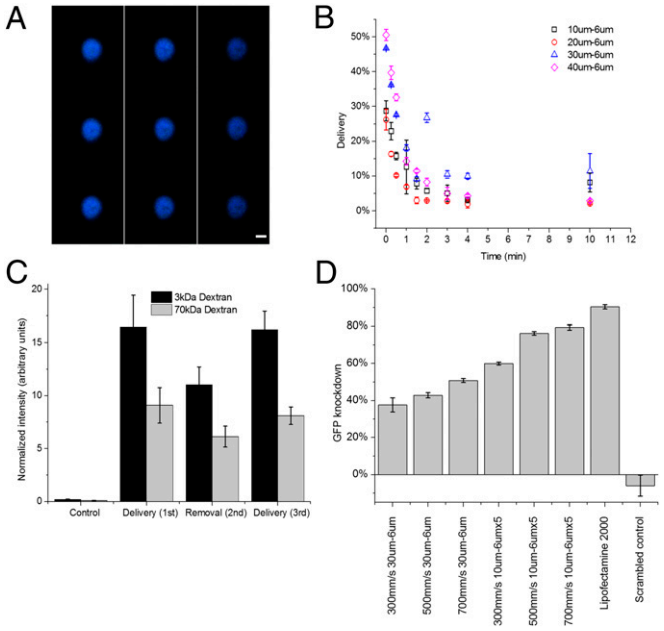

Fig. 3. Diffusive delivery mechanism. (*A*) Scans of different horizontal planes of a HeLa cell after the delivery of Cascade Blue-conjugated 3-kDa dextran, as measured by confocal microscopy. Note that 3-kDa dextran is small enough to enter the nuclear envelope (43). Scans read from top to bottom, and then left to right, where the top left is at $z = 6.98$ μm and bottom right is at $z = -6.7$ μm. (Scale bar: 6 μm.) (*B*) Live-cell delivery efficiency of 10 μm – 6 μm (□), 20 μm – 6 μm (○), 30 μm – 6 μm (△), and 40 μm – 6 μm (◇) devices. The time axis indicates the amount of time elapsed from initial treatment of cells before they were exposed to the target delivery solution. All results were measured by flow cytometry 18 h after treatment. (*C*) Average intensity of the delivered cell population normalized by untreated cells to control for autofluorescence. Fluorescein-conjugated 70-kDa dextran and Cascade Blue-conjugated 3-kDa dextran are delivered to the cell (cycles 1 and 3) and removed from the cell (cycle 2) in consecutive treatment cycles. The control represents cells that were only exposed to the delivery solution and not treated by the device. (*D*) Gene knockdown, as a function of device type and cell speed, in live destabilized GFP-expressing HeLa cells 18 h after the delivery of anti-eGFP siRNA at a delivery concentration of 5 μM. Lipofectamine 2000 was used as a positive control and scrambled controls were run at 500 mm/s on a 10 μm – 6 μm × 5. All data points were run in triplicate, and error bars represent 2 SDs.

with PBS and treated again in the absence of dextran (cycle 2), and finally treated a third time in the presence of 3- and 70-kDa dextran (cycle 3). The changes in normalized fluorescence intensity demonstrate a net diffusion of dextran into the cells during the first cycle, out of the cells during the second, and back in during the third (Fig. 3*C*). These results are thus consistent with the diffusive delivery hypothesis.

A simplified, 2D diffusion model was developed in COMSOL to simulate the passive diffusion of material into a cell across a porous membrane (Fig. S3 and *SI Note S1*). Using literature values for particle diffusivities inside and outside the cell cytoplasm (36), we were able to qualitatively re-create the experimental results of Fig. 3*C* with diffusion as the only mode of mass transfer. Moreover, by fitting our experimental data to this model, we estimate that the final concentration of delivery material in the cell cytosol is within 10–40% of the buffer concentration.

Furthermore, we demonstrated the functionality of the delivered materials by producing dosage-dependent, sequence-specific fluorescence knockdown in GFP-expressing HeLa cells (Fig. 3*D* and Fig. S2*C*). Although Lipofectamine 2000, a commercially available transfection reagent, achieved greater knockdown efficiencies, one must account for the prolonged delivery period of Lipofectamine particles (cells were incubated overnight) relative to the device's 2- to 5-min poration window. Device design and operating parameters were not optimized for siRNA delivery before performing these experiments.

Applicability Across Cell Types. To investigate the versatility of the technique, we assessed its ability to deliver model dextran molecules to several cell types that are traditionally difficult to transfect, especially immune cells and stem cells. Fluorescently labeled 70- and 3-kDa dextran were chosen for these experiments because they are similar in size to many protein and siRNA molecules respectively, easy to detect by flow cytometry, and have minimal surface binding effects as they are negatively charged. Using various device designs, we were able to deliver dextran molecules to newborn human foreskin fibroblasts (NuFFs) (Fig. 4*A*), primary murine dendritic cells (Fig. 4*B*), and embryonic stem cells (Fig. 4*C*). These experiments yielded minimal loss (<25%) in cell viability (Fig. 4 *A*–*C*), and preliminary results in murine embryonic stem cells indicate that the method does not induce differentiation (Fig. S4). In further studies, we isolated white blood cells (buffy coat layer) from murine blood by centrifugation and treated them with the device. B cells, T cells, and macrophages, as differentiated by antibody staining, indicated successful delivery of both 3- and 70-kDa dextran (Fig. 4 *D* and *E*, and Figs. S5–S7).

The preliminary evidence for a poration- and diffusion-based mechanism of delivery (Fig. 3 *A*–*C*) and the functionality of delivered materials (Fig. 3*D*) would indicate that these dextran

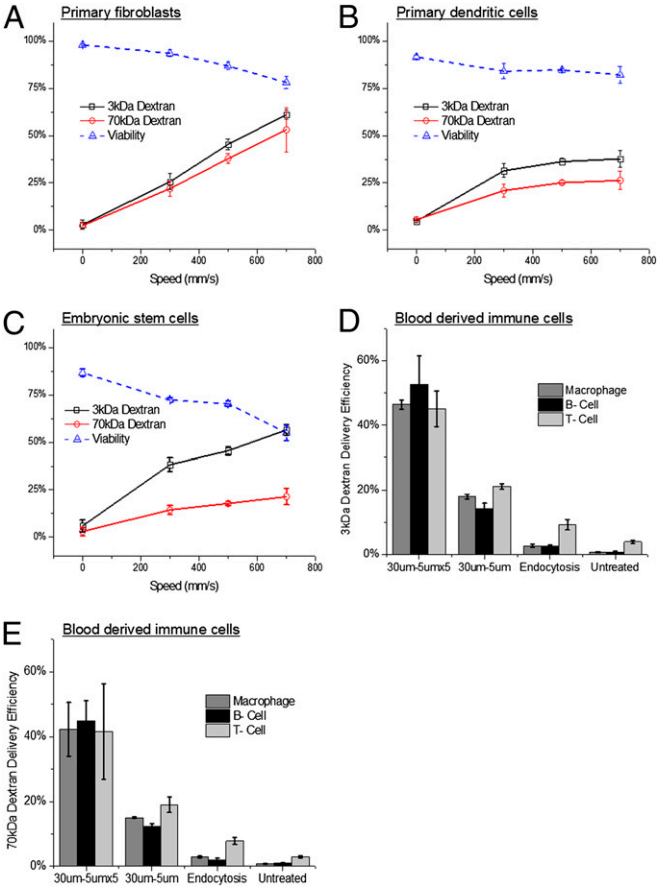

Fig. 4. Applicability across cell types. (*A*) Delivery efficiency and viability of NuFF cells treated with a 30 μm – 6 μm device to deliver 3- and 70-kDa dextran. (*B*) Delivery efficiency and viability of spleen-isolated, murine dendritic cells treated with a 10 μm – 4 μm device to deliver 3- and 70-kDa dextran. (*C*) Delivery efficiency and viability of murine embryonic stem cells treated with a 10 μm – 6 μm device to deliver 3- and 70-kDa dextran. (*D*) Delivery efficiency of 3-kDa and (*E*) 70-kDa dextran to B cells ($CD19^+$), T cells ($TCR\text{-}\beta^+$), and macrophages ($CD11b^+$) isolated from whole-mouse blood by centrifugation and treated by 30 μm – 5 μm and 30 μm – 5 μm × 5 devices at 1,000 mm/s. Three- and 70-kDa dextran were labeled with Cascade Blue and fluorescein, respectively. All data points were run in triplicate, and error bars represent 2 SDs.

delivery data should be representative of the expected cytosolic delivery efficiency for a protein or siRNA molecule of interest that is of similar size. Device designs have not been optimized for any of the aforementioned cell types, and we thus expect that further studies will yield improvements in viability and delivery efficiency. For a list of cell types that have successfully been treated using this technique and guidelines to designing new devices for specific cell types please refer to *SI Text* (Tables S1 and S2, and *SI Note S2*).

Enabling Delivery Platform. To illustrate our method's potential in addressing current delivery challenges, we conducted a number of proof-of-concept experiments in possible applications ranging from cell reprogramming (4) to carbon nanotube-based sensing (37). In addition to the application-specific materials detailed below, this method has demonstrated the successful delivery of Apolioprotein E, BSA, and GFP-plasmids.

The delivery of PEG1000-coated, 15-nm gold nanoparticles was verified by tunneling electron microscopy (TEM) of HeLa cells (Fig. 5 *A* and *B*). The nanoparticles appear to be mostly unaggregated and are not visibly sequestered into endosomes. In these images, we also observed tentative evidence for various defects in the cell cytoplasm, which could be the proposed holes responsible for delivery. We have also demonstrated high-throughput, noncytotoxic delivery of quantum dots directly to the cell cytosol (38)—a goal that current techniques have struggled to achieve. Furthermore, we were able to verify the successful delivery of carbon nanotubes (37) (encapsulated by a DNA oligonucleotide) by flow cytometry (Fig. 5*C*) and Raman spectroscopy (Fig. 5*D*). Antibodies to tubulin were also delivered (Fig. 5 *E* and *F*) using this technique, yielding a diffuse distribution throughout the cell that would be consistent with cytosolic delivery. The aforementioned materials are currently difficult to deliver to the cell cytosol and each material often requires a specialized modification to facilitate delivery. In our work, all four materials were delivered to HeLa cells using the same set of conditions on a 10 μm − 6 μm × 5 device.

Efficient delivery of proteins to primary cells could enable several therapeutic applications. A challenge in cell reprogramming (4), for example, is the inefficiency of current CPP-based protein delivery methods. We examined our ability to deliver four transcription factors (Oct4, Sox2, c-Myc, and Klf-4) to human fibroblast cells and compared our results to a CPP method (4) (Fig. 6*A*). Our results show that, in addition to not relying on endocytosis, which can leave much material trapped in endosomes, delivery by rapid mechanical deformation yields significantly higher delivery efficiency for all four proteins. Confocal imaging of cells treated by the device indicated that the transcription factors appear to successfully localize to the nucleus (Fig. 6*B*). Finally, to investigate the system's ability to affect gene transcription rates through the delivery of these proteins, we partially replicated a previous reprogramming study using commercially available (Stemgent) recombinant proteins (39). Briefly, NuFF cells were treated in the presence of recombinant c-Myc, Klf4, Oct4, and Sox2 for four cycles, spaced 2 d apart. The emergence of transformed colonies was monitored over a 1-mo period after the last treatment (Fig. 6*C*). The device was able to generate an average of 150 transformed colonies per plate relative to 11 and 2 colonies for electroporation and CPPs, respectively (Fig. S8). These colonies expressed embryonic stem cell markers, such as Oct4, SSEA-4, Tra-1-60, and Tra-1-81, and were capable of differentiating into all three germ layer cell types (Fig. 6 *D*–*G* and Fig. S8). These results suggest that transcription factors delivered by the microfluidic device are capable of affecting gene/protein expression more effectively than existing alternatives such as CPPs and electroporation.

Discussion

In the proposed intracellular delivery method, we hypothesize that transient holes are formed by rapid mechanical deformation of a cell as it passes through a microfluidic constriction. Our data support this notion by demonstrating diffuse cytosolic staining (Fig. 3*A*), siRNA functionality (Fig. 3*D*), and the bidirectional movement of material across the disrupted membrane (Fig. 3*C*).

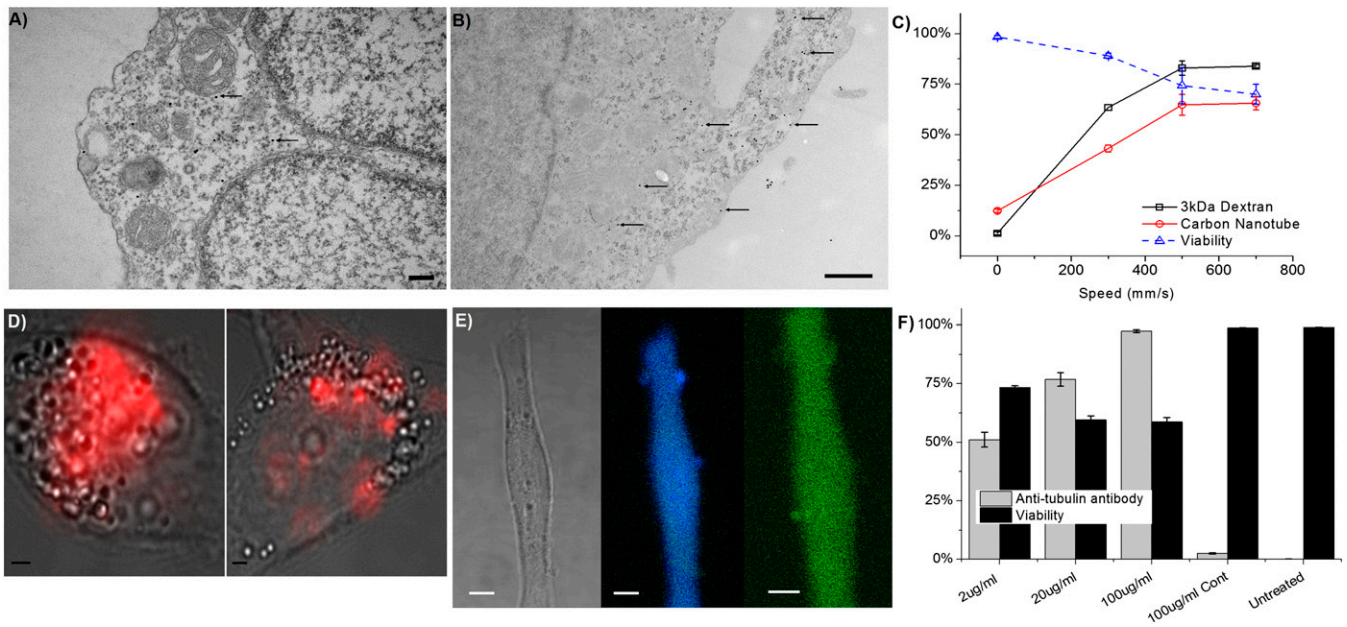

Fig. 5. Nanomaterial and antibody delivery. (*A* and *B*) TEM images of gold nanoparticles (some indicated by arrows) in cells fixed ~1 s after treatment by a 10 μm − 6 μm × 5 device (*SI Note S3*). (Scale bars: 500 nm.) (*C*) Delivery efficiency and viability of HeLa cells treated with a 10 μm − 6 μm × 5 device to deliver Cascade Blue-labeled 3-kDa dextran and Cy5-labeled, DNA-wrapped, carbon nanotubes. (*D*) Bright-field cell images overlaid with Raman scattering in the G-band (red) to indicate delivery of carbon nanotubes in treated cells (*Left*) vs. endocytosis (*Right*). (Scale bars: 2 μm.) (*E*) Fluorescent micrograph of a HeLa cell 18 h after delivery of Cascade Blue-labeled 3-kDa dextran (*Center*) and antibodies to tubulin with an Alexa Fluor 488 tag (*Right*). (Scale bars: 3 μm.) (*F*) Delivery efficiency and viability of HeLa cells treated with a 10 μm − 6 μm × 5 device, at 500 mm/s, to deliver Alexa Fluor 488-labeled anti-tubulin antibodies. Delivery efficiency at different antibody concentrations is compared with an endocytosis control at 100 μg/mL and untreated cells.

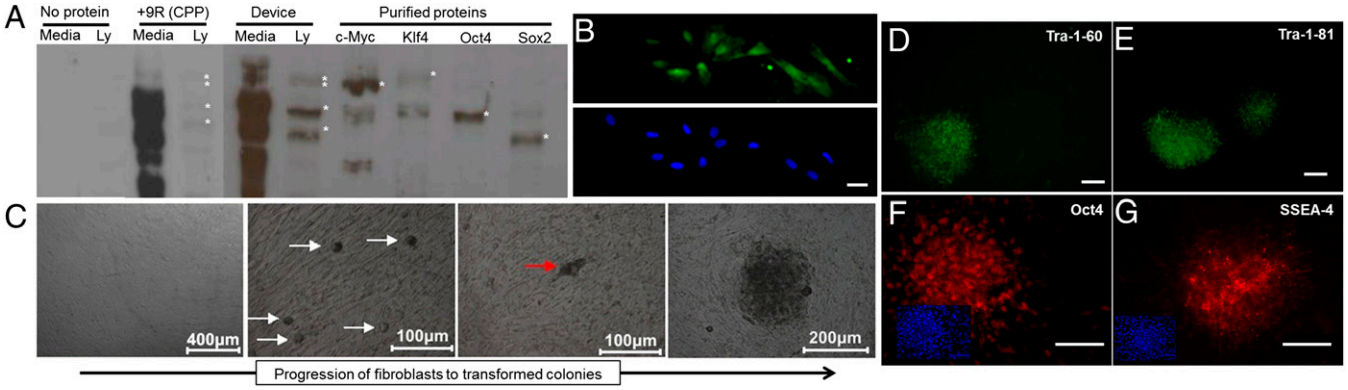

Fig. 6. Altering cell morphology and gene expression by cytosolic delivery of transcription factors. (*A*) A Western blot analysis of c-Myc, Klf4, Oct4, and Sox2 delivery to NuFF cells by cell-penetrating peptides versus a 10 μm – 6 μm device. Each of the four proteins has an additional nine arginine (9R) groups to facilitate uptake. The lysate (Ly) columns correspond to the protein content of cells that are washed and lysed, whereas the media columns correspond to the protein content of the media environment. (*B*) Confocal microscopy images of NuFF cells fixed after delivery of the reprogramming factors. The proteins are tagged using an Alexa 488-conjugated anti-FLAG antibody and the nucleus is stained by DAPI. (Scale bar: 15 μm.) (*C*) A progression of morphological changes from fibroblasts into colonies. The white arrows indicate potentially transformed cells. The red arrow points toward coalescing cells forming a colony. (*D–G*) Expression of the human embryonic stem cell marker Oct4, SSEA-4, Tra-1-60, and Tra-1-81 in transformed colonies (*SI Note S3*). Where appropriate, the small box represents a DAPI counterstain. (Scale bars: 100 μm.)

Moreover, this effect appears to be applicable across a wide range of cell types (Fig. 4), especially those that are difficult to treat with current methods, as we have demonstrated successful delivery in primary fibroblasts, embryonic stem cells, and a range of immune cells. In the future, by better understanding the effects of shear and compressive forces throughout the deformation process, one could potentially generate a family of devices with each optimized for a particular range of cell types and applications.

This delivery mechanism provides a number of potential advantages over existing methods. Similar to electroporation (22) and microinjection (28), it is a membrane disruption-based mechanism and hence does not rely on exogenous materials, chemical modification of payloads, or endocytotic pathways. In contrast to electroporation, however, it does not rely on electrical fields, which have had limited success in protein delivery (26), can damage target material (8), are dependent on the electrical charge of target material (40), or cause cytotoxicity (21). Indeed, current results have demonstrated relatively high viability in most applications and there is no underlying mechanism by which sensitive payloads, such as quantum dots or proteins, could be damaged. Direct comparisons to electroporation and CPP delivery of transcription factors further illustrated the system's advantage in improving biological activity.

The system could be an enabling research tool with its ability to deliver carbon nanotubes, gold nanoparticles, and antibodies (Fig. 5)—three materials that are difficult to deliver with current techniques. Such capabilities would significantly expand the research community's ability to probe intracellular processes by facilitating antibody and quantum dot staining of live cell structures/proteins and enabling the use of carbon nanotubes as a cytosolic molecular probe or chemical sensor. As a robust method of protein delivery, it could potentially be used for high-throughput screening of peptide/protein libraries because, unlike most CPP or nanoparticle-based techniques, this method is expected to be insensitive to protein structure and chemistry (41), does not rely on endocytotic pathways (14), and should not affect protein functionality (16). Moreover, it is possible that membrane disruption by rapid mechanical deformation occurs in vivo in response to certain stimuli or as part of a disease. Hence, investigating the phenomenon may prove relevant to better understanding disease mechanisms or physiological responses to trauma.

As a research tool, the microfluidic basis of our approach would allow it to be incorporated into a larger integrated system consisting of multiple pretreatment and posttreatment modules. At its current average throughput rate of 20,000 cells/s, the device could, for example, be placed in-line with a flow cytometry machine to sort cells or perform other analytical tasks immediately after delivery.

Finally, the technique could potentially enable novel approaches to therapy (Fig. 6). One can envision an approach whereby a patient's target cells are isolated from the blood or other tissue, treated by the device to deliver the desired therapeutic, and reintroduced into the body. Such an approach would take advantage of the potentially increased delivery efficiency of therapeutic macromolecules and could be safer than existing techniques because it would obviate the need for potentially toxic vector particles and would mitigate any potential side effects associated with reticuloendothelial clearance and off-target delivery.

Conclusion

In summary, we have detailed a method for cytosolic delivery that relies on the rapid mechanical deformation of a cell to induce transient membrane disruption. This technique has demonstrated the potential to deliver a broad range of materials, some of which are challenging to use with current methods, to a variety of difficult-to-transfect cell types, including stem cells and immune cells. By providing flexibility in application and obviating the need for exogenous materials or electrical fields, this method could potentially enable new avenues of disease research and treatment. Indeed, our work has demonstrated this system's ability to deliver carbon nanotubes, quantum dots (38), and antibodies to live cells—applications that could enable new sensing and imaging modalities—and we have illustrated the system's superior performance, relative to current methods, in applications such as transcription factor delivery for reprogramming.

Materials and Methods

Device Fabrication and Mounting System. The silicon-based devices are fabricated at the Massachusetts Institute of Technology microfabrication facility using photolithography and deep reactive ion etching techniques. In this process, 6″ silicon wafers with a 450-μm thickness are treated with hexamethyldisilazane, spin coated with photoresist (OCG934; FujiFilm) for 60 s at 3,000 rpm, exposed to UV light (EV1; EVG) through a chrome mask with the constriction channel design, and developed in AZ405 (AZ Electronic Materials) solution for 100 s. After 20 min of baking at 90 °C, the wafer is etched by deep reactive ion etching (SPTS Technologies) to the desired depth (typically 15 μm). The process is repeated on the opposite side of the wafer (i.e., the one not containing the etched channels) using a different mask, which contains the access hole patterns, and using a thicker photoresist AZ9260 (AZ Electronic Materials). Wet oxidation is then used to grow 100–200 nm of silicon oxide before the wafer is anodically bonded to a Pyrex wafer and diced into individual devices. Before each experiment, devices are

visually inspected and mounted onto a holder with inlet and outlet reservoirs (all designed in-house and produced by Firstcut). These reservoirs interface with the device using Buna-N O-rings (McMaster-Carr) to provide proper sealing. The inlet reservoir is connected to a home-made pressure regulator system using Teflon tubing to provide the necessary driving force to push material through the device. Our current system can only accommodate pressures up to 120 psi.

Dendritic Cell Isolation. Murine dendritic cells were isolated from the spleen of BL6 mice (Taconic) using a CD11c-positive selection MACS sort (Miltenyi Biotec).

Delivery Procedure. To perform an experiment, cells are first suspended in the desired delivery buffer [growth medium, PBS, or PBS supplemented with 3% FBS and 1% F-68 Pluronics (Sigma)], mixed with the desired delivery material, and placed in the device's inlet reservoir. This reservoir is connected to a compressed air line controlled by a regulator, and the selected pressure (0–70 psi) is used to drive the fluid through the device. Treated cells are then collected from the outlet reservoir. Cells are incubated at room temperature in the delivery solution for 5–20 min after treatment to ensure hole closure before being subjected to any further treatment.

Delivery Materials. To deliver fluorescently labeled dextran molecules (Invitrogen), the experiments were conducted as described above such that the delivery buffer contained 0.1–0.3 mg/mL dextran. GFP knockdown is measured as the percentage reduction in a cell population's average fluorescence intensity relative to untreated controls. Lipofectamine 2000 plus siRNA particles were prepared by combining 1 μg of siRNA with 1 μL of Lipofectamine 2000 reagent in 100 μL of PBS.

Confocal Microscopy. Confocal images were taken using techniques described previously (38).

Reprogramming Factor Purification by FLAG. FLAG-tagged reprogramming factors (c-Myc, Klf4, Oct4, and Sox2) were generated as previously described (4).

Western Blotting. After treatment by the device, cells were seeded on to a culture plate. After 4 h, the culture media, which contains any undelivered proteins, was collected and processed as previously described (4).

Transcription Factor Delivery Studies. We replicated the delivery procedure illustrated by a previous group to generate pluripotent stem cells using recombinant proteins with a CPP modification (39). Briefly, 10^5 cells (per sample) were treated by the device (30 μm – 6 μm at 500 mm/s) or Neon Transfection System (Invitrogen) in the presence of 80 μg/mL of each transcription factor (Stemgent). Treatment was repeated once every 2 d with a media change every day as previously described. After treatment was complete, the cells were transferred to mTeSR-1 media (Stemcell) and colony counts were performed at 16–18 d (device case) or 30–31 d (nucleofection and CPP cases) after treatment. The difference in counting time reflects the earlier emergence of colonies in the device case.

Raman Spectroscopy. The home-built Raman system was used as previously described (42).

ACKNOWLEDGMENTS. We thank T. Shatova for helpful discussion on experimental design and data analysis. We thank J. Naffin and Prof. G. Petsko for their guidance in designing/performing protein delivery experiments. Nicki Watson of the Whitehead Institute assisted in TEM imaging. The assistance and expertise of G. Paradis, the personnel of the flow cytometry core at the Koch Institute, and the staff of the Microsystems Technology Laboratory at Massachusetts Institute of Technology are gratefully acknowledged. This work was supported by National Institutes of Health Grants RC1 EB011187-02, DE013023, DE016516, EB000351, and partially by National Cancer Institute Cancer Center Support (Core) Grants P30-CA14051 and MPP-09Call-Langer-60.

1. Schaffert D, Wagner E (2008) Gene therapy progress and prospects: Synthetic polymer-based systems. *Gene Ther* 15(16):1131–1138.
2. Whitehead KA, Langer R, Anderson DG (2009) Knocking down barriers: Advances in siRNA delivery. *Nat Rev Drug Discov* 8(2):129–138.
3. Leader B, Baca QJ, Golan DE (2008) Protein therapeutics: A summary and pharmacological classification. *Nat Rev Drug Discov* 7(1):21–39.
4. Kim D, et al. (2009) Generation of human induced pluripotent stem cells by direct delivery of reprogramming proteins. *Cell Stem Cell* 4(6):472–476.
5. Dhar S, Daniel WL, Giljohann DA, Mirkin CA, Lippard SJ (2009) Polyvalent oligonucleotide gold nanoparticle conjugates as delivery vehicles for platinum(IV) warheads. *J Am Chem Soc* 131(41):14652–14653.
6. Jiang Z-X, Zhang Z-Y (2008) Targeting PTPs with small molecule inhibitors in cancer treatment. *Cancer Metastasis Rev* 27(2):263–272.
7. Derfus AM, Chan WCW, Bhatia SN (2004) Intracellular delivery of quantum dots for live cell labeling and organelle tracking. *Adv Mater* 16(12):961–966.
8. Michalet X, et al. (2005) Quantum dots for live cells, in vivo imaging, and diagnostics. *Science* 307(5709):538–544.
9. Dahan M, et al. (2003) Diffusion dynamics of glycine receptors revealed by single-quantum dot tracking. *Science* 302(5644):442–445.
10. Slowing II, Trewyn BG, Lin VSY (2007) Mesoporous silica nanoparticles for intracellular delivery of membrane-impermeable proteins. *J Am Chem Soc* 129(28):8845–8849.
11. Pack DW, Hoffman AS, Pun S, Stayton PS (2005) Design and development of polymers for gene delivery. *Nat Rev Drug Discov* 4(7):581–593.
12. Zabner J (1997) Cationic lipids used in gene transfer. *Adv Drug Deliv Rev* 27(1):17–28.
13. Verma A, et al. (2008) Surface-structure-regulated cell-membrane penetration by monolayer-protected nanoparticles. *Nat Mater* 7(7):588–595.
14. Heitz F, Morris MC, Divita G (2009) Twenty years of cell-penetrating peptides: From molecular mechanisms to therapeutics. *Br J Pharmacol* 157(2):195–206.
15. Duan H, Nie S (2007) Cell-penetrating quantum dots based on multivalent and endosome-disrupting surface coatings. *J Am Chem Soc* 129(11):3333–3338.
16. Yan M, et al. (2010) A novel intracellular protein delivery platform based on single-protein nanocapsules. *Nat Nanotechnol* 5(1):48–53.
17. Shi Kam NW, Jessop TC, Wender PA, Dai H (2004) Nanotube molecular transporters: Internalization of carbon nanotube-protein conjugates into mammalian cells. *J Am Chem Soc* 126(22):6850–6851.
18. Varkouhi AK, Scholte M, Storm G, Haisma HJ (2011) Endosomal escape pathways for delivery of biologicals. *J Control Release* 151(3):220–228.
19. Waehler R, Russell SJ, Curiel DT (2007) Engineering targeted viral vectors for gene therapy. *Nat Rev Genet* 8(8):573–587.
20. Hu Y-C (2008) Baculoviral vectors for gene delivery: A review. *Curr Gene Ther* 8(1):54–65.
21. Li S (2004) Electroporation gene therapy: New developments in vivo and in vitro. *Curr Gene Ther* 4(3):309–316.
22. Fox MB, et al. (2006) Electroporation of cells in microfluidic devices: A review. *Anal Bioanal Chem* 385(3):474–485.
23. Miller DL, Pislaru SV, Greenleaf JE (2002) Sonoporation: Mechanical DNA delivery by ultrasonic cavitation. *Somat Cell Mol Genet* 27(1–6):115–134.
24. Prentice HL (1992) High efficiency transformation of Schizosaccharomyces pombe by electroporation. *Nucleic Acids Res* 20(3):621.
25. Prechtel AT, Turza NM, Theodoridis AA, Kummer M, Steinkasserer A (2006) Small interfering RNA (siRNA) delivery into monocyte-derived dendritic cells by electroporation. *J Immunol Methods* 311(1–2):139–152.
26. Lambert H, Pankov R, Gauthier J, Hancock R (1990) Electroporation-mediated uptake of proteins into mammalian cells. *Biochem Cell Biol* 68(4):729–734.
27. Marrero MB, Schieffer B, Paxton WG, Schieffer E, Bernstein KE (1995) Electroporation of pp60c-src antibodies inhibits the angiotensin II activation of phospholipase C-gamma 1 in rat aortic smooth muscle cells. *J Biol Chem* 270(26):15734–15738.
28. Zhang Y, Yu L-C (2008) Microinjection as a tool of mechanical delivery. *Curr Opin Biotechnol* 19(5):506–510.
29. Luo D, Saltzman WM (2000) Synthetic DNA delivery systems. *Nat Biotechnol* 18(1):33–37.
30. Clarke MS, McNeil PL (1992) Syringe loading introduces macromolecules into living mammalian cell cytosol. *J Cell Sci* 102(Pt 3):533–541.
31. Hallow DM, et al. (2008) Shear-induced intracellular loading of cells with molecules by controlled microfluidics. *Biotechnol Bioeng* 99(4):846–854.
32. el-Fouly MH, Trosko JE, Chang C-C (1987) Scrape-loading and dye transfer. A rapid and simple technique to study gap junctional intercellular communication. *Exp Cell Res* 168(2):422–430.
33. Rejman J, Bragonzi A, Conese M (2005) Role of clathrin- and caveolae-mediated endocytosis in gene transfer mediated by lipo- and polyplexes. *Mol Ther* 12(3):468–474.
34. Pastan IH, Willingham MC (1981) Receptor-mediated endocytosis of hormones in cultured cells. *Annu Rev Physiol* 43:239–250.
35. McNeil PL, Steinhardt RA (2003) Plasma membrane disruption: Repair, prevention, adaptation. *Annu Rev Cell Dev Biol* 19:697–731.
36. Periasamy N, Verkman AS (1998) Analysis of fluorophore diffusion by continuous distributions of diffusion coefficients: Application to photobleaching measurements of multicomponent and anomalous diffusion. *Biophys J* 75(1):557–567.
37. Heller DA, Baik S, Eurell TE, Strano MS (2005) Single-walled carbon nanotube spectroscopy in live cells: towards long-term labels and optical sensors. *Adv Mater* 17(23):2793–2799.
38. Lee J, et al. (2012) Nonendocytic delivery of functional engineered nanoparticles into the cytoplasm of live cells using a novel, high-throughput microfluidic device. *Nano Lett* 12(12):6322–6327.
39. Zhou H, et al. (2009) Generation of induced pluripotent stem cells using recombinant proteins. *Cell Stem Cell* 4(5):381–384.
40. Prausnitz MR, et al. (1993) A quantitative study of electroporation showing a plateau in net molecular transport. *Biophys J* 65(1):414–422.
41. Xu Y, Du Y (2003) Effect of molecular structure of chitosan on protein delivery properties of chitosan nanoparticles. *Int J Pharm* 250(1):215–226.
42. Kang JW, et al. (2011) Combined confocal Raman and quantitative phase microscopy system for biomedical diagnosis. *Biomed Opt Express* 2(9):2484–2492.
43. Alberts B, Johnson A, Lewis J (2002) *Molecular Biology of the Cell* (Garland Science, New York), 4th Ed.